Phase and Nanostructure Information by Plasmon Excitation with Auger Electrons

Hans Joachim Steffen (a) and Siegfried Hofmann (b)

(a) *Fachhochschule Mannheim, University of Applied Sciences, Mannheim, Germany*
(b) *National Research Institute for Metals, Tsukuba, Japan*

(Received: Jan. 30, 1997 Accepted: Feb. 20, 1997)

Abstract

Plasmon energies contain useful information not only about the electron density but also about the shape and size of the excited volume. The respective relations principally enable characterization of different phases with their specific electron densities and morphologies, and, in addition, characterization of the structure of heterogeneous phase mixtures. This study presents a new approach to reveal the chemical states of elements along with the existing phase structure in heterogeneous materials from Auger spectra measured at different kinetic energies. The concept of this method is demonstrated using Auger measurements of silicon samples implanted with carbon ions and with oxygen ions. In the latter case, analysis of the plasmon energy loss tails shows the existence of bulk-like silicon crystals embedded in a buried heterogeneous silicon oxide layer. In the former case, the existence of small silicon carbide precipitates with an average size between 0.5 and 3 nm in a carbon-silicon phase is clearly indicated. It is concluded that electron spectroscopy can be successfully applied for the characterization of heterogeneous materials with embedded nanoparticles in the matrix.

1. Introduction

Although Auger valence band transitions and photoelectron emissions are sensitively influenced by the chemical state of atoms, spectral line shape analyses in Auger electron spectroscopy (AES) and X-ray photoelectron spectroscopy (XPS) neither reveal phase formation nor the existence of a heterogeneous phase mixture in covalent bound solids. This is due to the discrete molecular orbital overlap and local nature of chemical bonds in semiconductors which may contain different heteronuclear bonds in a homogeneous mixture. For example, the surface reaction of silicon with a small amount of atomic oxygen results in the formation of a certain fraction of oxidized silicon atoms at the surface. However, the observed chemical shift in electron spectra does not necessarily indicate the formation of an oxide phase. In fact, phase formation is related to micro- or submicroscopic matter with uniform physical properties which naturally does not exclude different chemical states of atoms. Therefore, it is imperative to adopt a probe with finite spatial resolution to characterize phases and phase distributions in contrast to the use of atomic Auger and photoelectron emissions in conventional AES and XPS.

This limitation of electron spectroscopy can be mastered if the average electron density of a certain volume of matter is used to discriminate and characterize phases. According to the jellium model for solids with quasifree electrons the response of the electron gas to an external electric field or incident charged particle is a collective oscillation of the electron density at a characteristic frequency. Consequently, these electron density dependent plasma oscillations describe the state of matter and represent a significant phase property of the characteristic excitation volume[1]. Since in many cases inelastic electron scattering is dominated by plasmon excitations, electron spectra generally contain information about plasmon energies due to distinct plasmon energy loss intensities near Auger and photoemission lines at lower kinetic energy. For many semiconductor and insulator materials these plasmon energies are proportional to the square root of the electron density according to the well-known expression for the plasma-resonance energy of a free electron gas[2]. Moreover, the plasmon energy depends also on the shape and size of the excited volume as well as the oscillation mode[3]. The resulting additional numeric factor which influences the plasmon energy varies from about $1/\sqrt{3}$ for spherical nanometer-sized particles to $1/\sqrt{2}$ for very large particles and material surfaces and equals 1 for excitations of bulk plasmons. Therefore, plasmon excitations which occur for Auger electrons and photoelectrons after the emission at a distance of the inelastic mean free

path to the atomic site of ionization, may reveal the local and site-dependent state of matter. This study represents a new approach to obtain phase and nanostructure information about heterogeneous silicon materials from careful analysis of the plasmon energy loss tails of the low energy Si LVV and high energy KLL Auger lines and significantly refines the quantitative chemical state analysis by valence band AES[4,5].

2. Experimental

AES depth profiling was performed for two different (100)-silicon samples A and B. Sample A was internally oxidized by a high-energy oxygen implantation at 2 MeV and 400 °C and a subsequent annealing at 1300 °C for 12 hours. Transmission electron microscopy proved the formation of a heterogeneous buried silicon oxide layer at a depth of ca. 2 μm with large silicon crystal inclusions (diameter of ca. 100 nm) which are concentrated at the inner zone of the oxide layer. Sample B was at first amorphized in the surface region by a high-energy and low-dose Ge^+-ion implantation and then subjected to a C^+-ion implantation at 25 keV and room temperature with a dose density of 1×10^{17} ions/cm^2. The measured carbon concentration profile agrees fairly well with a calculated Pearson-4 distribution and peaks around 60 nm. Sputtering was carried out with a 3 keV Ar^+ ion beam at an incidence angle of 54° to the surface normal. The ion beam was rastered over an area of about 1 mm^2 resulting in an ion current density of ca. 140 mA/cm^2. The samples were rotating during ion sputtering to give a better depth resolution. Under these conditions a sputter rate of ca. 0.29 nm/s for silicon and 0.52 nm/s for thermally grown SiO_2 were measured to convert the sputter time into a depth scale. The Auger transitions were excited with a rastering electron beam (5 keV and 90 nA) and measured with a hemispherical analyzer at an electron emission angle of 30° to the surface normal. The analyzer was collecting electrons from a sample area of ca. 69×56 μm and operating at a constant energy resolution of 0.4 eV for the Si LVV (92 eV) and 1 eV for the Si $KL_{23}L_{23}$ (1616 eV) transitions. The spectra were acquired in the pulse-counting mode with a collection time of 2 s/channel and subjected to a nine-point smoothing and five-point differentiation for Si LVV and to a five-point smoothing for Si $KL_{23}L_{23}$.

3. Results and Discussion

The Si $KL_{23}L_{23}$ spectra including the inelastic energy loss parts in Fig. 1 reveal that the buried silicon oxide layer of sample A contains a heterogeneous inner zone with bulk-like oxide and silicon phases at a depth of 1946 nm. In contrast to homogeneous silicon oxide at 2042 nm (no significant element silicon peak, one plasmon energy loss peak), the spectrum at 1946 nm shows three distinct plasmon energy loss peaks at 17 and 23 eV lower kinetic energy with respect to the Si^0 and Si^{4+} peak positions. This is the consequence of simultaneous plasmon excitations in both phases silicon and silicon oxide requiring 17 and 23 eV respectively by Auger electrons from Si^0. The inelastic mean free path (IMFP) of Auger electrons at 1616 eV from Si^0 of the embedded silicon crystals is about 3 nm which enables also the excitation of plasmons within the oxide layer after passing the phase boundary. Hence, plasmon energy loss peaks give evidence for the existence

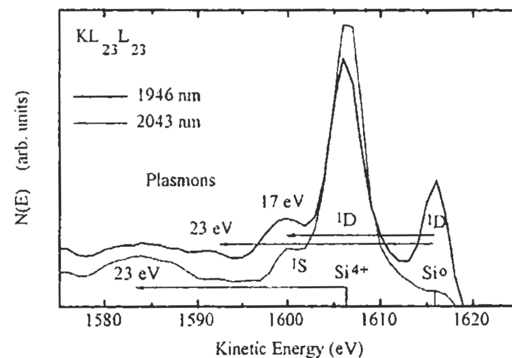

Fig. 1 Si $KL_{23}L_{23}$ spectra of sample A at sputtering depths of 1946 and 2043 nm. The spectrum at 1946 nm represents the heterogeneous inner zone of the buried silicon oxide layer with embedded silicon crystals. The spectrum at 2043 nm represents the homogeneous oxide layer near the lower oxide-silicon substrate interface. The energy positions of the $KL_{23}L_{23}$ line for the fully oxidized Si^{4+} and elemental Si^0 state are indicated and peak assignments are shown. The arrows along with the respective energy values characterize plasmon energy losses for Auger electrons from oxidized and elemental silicon.

of phases corresponding to their characteristic excitation energies.

In spite of the general phase susceptibility of conventional reflective electron energy loss spectroscopy it hardly discloses the morphology of heterogeneous systems, e. g. continuous and discontinuous phases can usually not be distinguished but only the existence of different phases. This is the consequence of uniform

plasmon excitations within the probe volume of the primary electron beam which precludes a localization of inelastic scattering events and, therefore, an assignment of characteristic plasmon energies to each sample region. This restriction is partially circumvented if Auger electrons are applied as a local probe because they excite plasmons at defined distances from chosen emitters. Hence, if the site of electron emission is known and intrinsic energy losses during Auger transitions are neglected, then IMFP determines the site of plasmon excitation.

Consequently, different Auger electrons, like LVV and $KL_{23}L_{23}$ electrons of Si, probe a volume with different radii around the emitter according to the kinetic-energy dependence of IMFP. The merit of this concept is demonstrated with Fig. 2 which shows Auger lines along with the related characteristic energy losses of Si, 6H-SiC and amorphous SiC reference samples (bottom frame). These loss peaks are caused by Si $KL_{23}L_{23}$ electrons which travel in Si and SiC ca. 3.5 and 2.8 nm, respectively, before plasmon excitations occur. Therefore, the plasmon energies of ca. 17 and 23 eV reveal the existence of Si and SiC phase, respectively, in the vicinity of Si atoms.

Unlike this trivial case of single phase materials, the sequence of Si $KL_{23}L_{23}$ spectra (top frame) of carbon-implanted silicon reveals the formation of a homogeneous silicon-carbon solution around Si according to the depth-dependent plasmon peak shift. The depth-dependent plasmon energy is obviously a function of carbon concentration. But a conclusive statement about the structure of the carbon implantation zone can only be obtained by the following. In contrast to high energy $KL_{23}L_{23}$ electrons, low energy LVV electrons with a IMFP of only 0.5 nm in Si and SiC probe the immediate vicinity of Si atoms. The corresponding loss part of the LVV spectra in dependence on sputtering depth is shown in Fig. 3 in comparison with the spectrum of crystalline 6H-SiC.

The plasmon peak at 75 eV for pure Si shifts to

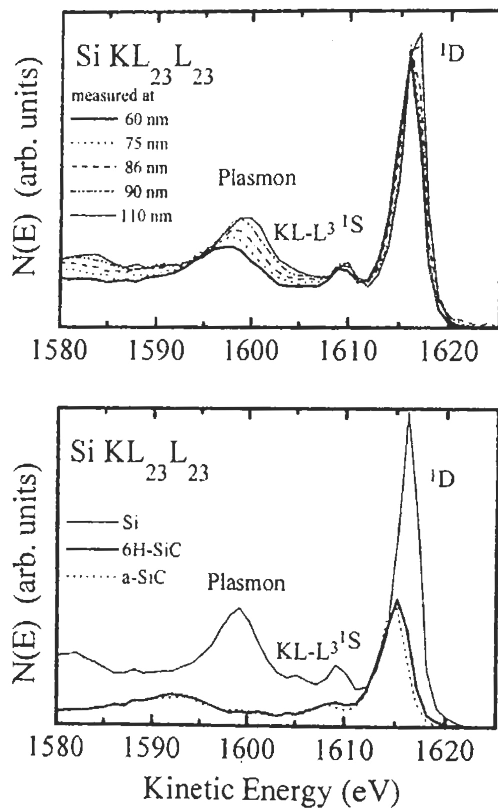

Fig. 2 Bottom frame: Si $KL_{23}L_{23}$ spectra of crystalline Si, 6H-SiC and a-SiC with peak assignments. The plasmon peaks are caused by $KL_{23}L_{23}$ electrons which leave behind a ^1D-Si atom and suffer energy losses of ca. 17 eV in Si and 23 eV in SiC. Please note that there is only a small chemical shift of the ^1D-line in SiC compared to Si. Top frame: Si $KL_{23}L_{23}$ spectra of carbon-implanted Si at different sputtering depths. The plasmon loss peak shifts relative to the ^1D peak in dependence on the carbon concentration which is at maximum around 60 nm.

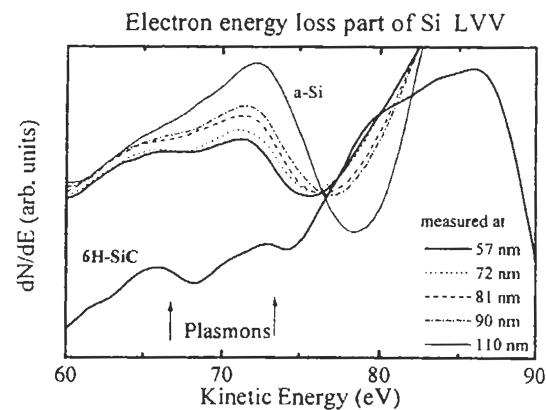

Fig. 3 Electron energy loss part (60-90 eV) of the derived Si LVV spectra at different indicated depths. The plasmon loss peak shifts relative to the LVV peak at ca. 92 eV in dependence on the carbon concentration. Note that a distinct peak at 67 eV emerges in correlation with increasing carbon concentration which is at maximum around 60 nm. For comparison, the spectrum of 6H-SiC with peaks at ca. 67 and 73 eV is shown. These can be assigned to bulk and surface plasmons with energies of ca. 23 and 17 eV, respectively.

lower kinetic energy as a function of the depth-dependent carbon concentration similar to the sequence of spectra in Fig. 2. A distinct peak emerges at ca. 67 eV for spectra measured around 60 nm at high carbon concentration. A similar more intense peak is also observed in the 6H-SiC reference spectrum and accounts most likely for a 23 eV energy loss of Si LVV electrons.

Conclusively, the excitation of 23 eV plasmons by low energy Auger electrons manifests the growth of SiC-like regions with an average domain size larger than the IMFP of 0.5 nm. Apparently, the silicon-carbon matrix at high carbon concentration can not be considered as homogeneous on the nanometer scale but local carbon enrichment may result in SiC particles. An upper limit of the average particle size of ca. 3 nm can be qualitatively rationalized regarding the absence of 23 eV plasmon losses in the $KL_{23}L_{23}$ spectra. The likelihood for plasmon excitations within the particles of diameter <d> by $KL_{23}L_{23}$ electrons is anticipated to be much smaller than for LVV electrons as illustrated in Fig. 4. Therefore, we assume an average SiC particle size between 0.5 and 2.8 nm according to the $IMFP_s$ of Si Auger electrons.

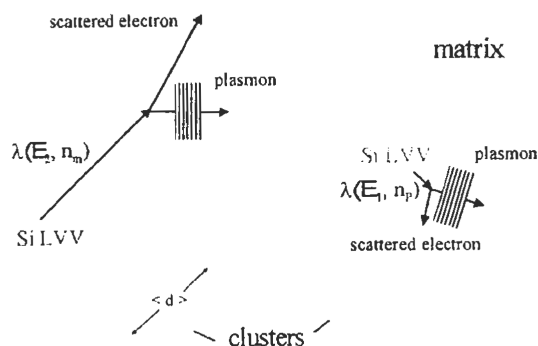

Fig. 4 Scheme of the inhomogeneous carbon-implanted silicon matrix with electron density n_m and SiC nanoscale particles (precipitates) with electron density n_p to clarify the plasmon loss peaks in Fig. 2 and 3. The IMFP of Si $KL_{23}L_{23}$ electrons with E_2=1616 eV in the matrix is ca. 3.5 nm ($\lambda(E_2, n_m)$) and larger than the average particle diameter <d>. Therefore, plasmon excitations in SiC at a resonance frequency corresponding to n_p is not very likely compared to plasmon excitations in the silicon-carbon matrix. In contrast, Si LVV electrons with E_1=90 eV suffer inelastic scattering after travelling only $\lambda(E_1, n_p)$=0.5 nm and cause plasmon excitations in both the matrix and particles at resonance frequencies corresponding to n_m and n_p.

4. Conclusion

Both Si LVV and $KL_{23}L_{23}$ spectra reveal plasmon energy loss peaks which shift in dependence on the chemical composition and electron density of the excited volume. The corresponding plasmon energy characterizes the state of matter and identifies phases in the vicinity of the Auger electron emitters. In the first case of oxygen-implanted and annealed silicon the existence of a heterogeneous silicon oxide layer with bulk-like silicon inclusions could be demonstrated by distinct plasmon energy loss peaks originating from Auger transitions in oxidized and elemental silicon. In the second case it was demonstrated how electron energy loss parts of the low- and high-energy Si Auger spectra may characterize heterogeneous materials or phases on the nanometer scale owing to the electron density-dependent plasmon energies and kinetic energy-dependent $IMFP_s$. Particularly, the average size of small precipitates or particles between certain limits can be assessed. Carbon implantation into silicon results in a homogeneous silicon-carbon matrix but fine-dispersed SiC particles with an average size between 0.5 and 3 nm have most likely formed at high carbon concentrations. This work represents a preliminary study of the response of nanostructured materials to a primary electron beam. Our future work will focus especially on plasmon excitations in nanomaterials and their effects on electron spectra.

References

1. L. Onsager, Phys. Rev. **54** (1938) 554.
2. C. Kittel, Introduction to Solid State Physics, John Wiley, New York, 1976.
3. F. Fujimoto, K. Komaki and K. Ishida, J. Phys. Soc. Japan **23** (1967) 1186.
4. H. J. Steffen, Thin Solid Films **253** (1994) 269.
5. S. Hofmann and J. Steffen, Surf. Interface Anal. **14** (1989) 59.